SUPPLEMENTARY APPENDIX

The interactome of the N-terminus of band 3 regulates red blood cell metabolism and storage quality

Aaron Issaian,[1] Ariel Hay,[2] Monika Dzieciatkowska,[1] Domenico Roberti,[3] Silverio Perrotta,[3] Zsuzsanna Darula,[4] Jasmina Redzic,[1] Micheal P. Busch,[5] Grier P. Page,[6] Stephen C. Rogers,[7] Allan Doctor,[7] Kirk C. Hansen,[1] Elan Z. Eisenmesser,[1] James C. Zimring[2] and Angelo D'Alessandro[1]

[1]Department of Biochemistry and Molecular Genetics, University of Colorado Denver – Anschutz Medical Campus, Aurora, CO, USA; [2]University of Virginia, Charlottesville, VA, USA; [3]Università della Campania "L. Vanvitelli", Naples, Italy; [4]Laboratory of Proteomics Research, Biological Research Center, Szeged, Hungary; [5]Vitalant Research Institute, San Francisco, CA, USA; [6]RTI International, Pittsburgh, PA, USA and [7]University of Maryland, Baltimore, MD, USA

©2021 Ferrata Storti Foundation. This is an open-access paper. doi:10.3324/haematol.2020.278252

Received: December 24, 2020.

Accepted: February 26, 2021.

Pre-published: May 13, 2021.

Correspondence: *ANGELO D'ALESSANDRO* - angelo.dalessandro@ucdenver.edu

JAMES C ZIMRING - jcz2k@virginia.edu

Supplementary Material for the article

The interactome of the N-terminus of band 3 regulates red blood cell metabolism and storage quality

Aaron Issaian,[1] Ariel Hay,[2] Monika Dzieciatkowska,[1] Domenico Roberti,[3] Silverio Perrotta,[3] Zsuzsanna Darula,[4] Jasmina Redzic,[1] Micheal P. Busch,[5] Grier Page,[6] Stephen C Rogers,[7] Allan Doctor,[7] Kirk C. Hansen,[1] Elan Z Eisenmesser,[1] James C Zimring,[2,*] Angelo D'Alessandro,[1*]

1) Department of Biochemistry and Molecular Genetics, University of Colorado Denver – Anschutz Medical Campus, Aurora, CO, USA;
2) University of Virginia, Charlotesville, VA, USA
3) Università della Campania "L. Vanvitelli", Naples, Italy
4) Laboratory of Proteomics Research, Biological Research Center of the Hungarian Academy of Sciences, H-6701 Szeged, Hungary.
5) Vitalant Research Institute, San Francisco, CA, USA
6) RTI International, Pittsburgh, PA, USA
7) University of Maryland, Batlimore, MD, USA

***Corresponding authors:**

Angelo D'Alessandro, PhD
Department of Biochemistry and Molecular Genetics
University of Colorado Anschutz Medical Campus
12801 East 17th Ave., Aurora, CO 80045
Phone # 303-724-0096
E-mail: angelo.dalessandro@ucdenver.edu

James C Zimring, MD PhD
Department of Pathology
University of Virginia, Charlottesville, VA, USA
345 Crispell Drive (MR6), Room 3523, Charlottesville, VA 22903
Phone: #434-924-2427
Email: jcz2k@virginia.edu

SUPPLEMENTARY MATERIAL

TABLE OF CONTENTS

Methods

Animal studies with mice All the animal studies described in this manuscript were reviewed and approved by the University of Virginia Institutional Animal Care and Use Committee (protocol n: 4269). Band 3 mouse founders, including huB3, HA Del and BS KO mice – originally generated by Low's group[1] - were acquired from the National Institutes of Health mouse embryo repository and were bred with C57BL/6 females. The use of Ubi-GFP and HOD mice have been previously described in prior work from our group.[2] Whole blood was drawn by cardiac puncture as a terminal procedure for the mice. Blood was snap frozen in liquid nitrogen and storaged at -80ºC until subsequent analysis. For transfusion studies, fresh RBCs (never frozen) were used.

Band 3 Neapolis RBCs (100 ul) were obtained from a subject carrying a rare mutation resulting in the lack of amino acids 1-11 in the N-terminus of band 3, as extensively described by Perrotta et al.[3]

Methylene blue treatments RBCs from WT and band 3 KO mice were incubated with methylene blue (100 uM, Sigma Aldrich) at 37°C for 1h, as described,[4] prior to metabolomics analyses.

Storage under blood bank conditions RBCs from the four main strains investigated in this study, along with 13 different mouse strains described before[5] were collected, processed, stored, transfused and post-transfusion recovery was determined as previously described.[5]

Tracing experiments with labeled glucose, citrate, glutamine, arachidonic acid and methionine RBCs from all the mouse strains investigated in this study (100 ul) or RBC lysates from healthy donor volunteers (n=3) or the individual carrying band 3 Neapolis RBCs were incubated at 37ºC for 1h in presence of 1,2,3-$^{13}C_3$-glucose (5 mM – Cambridge Isotopes – product no. CLM-4673), prior to determination of lactate isotopologues +2/+3 (as markers of pentose phosphate pathway to glycolysis fluxes), as described.[6] Additional tracing experimetns were performed by incubating RBCs with $^{13}C^{15}N$ -methionine (1 mM – Sigma Aldrich – product no. 608106), $^{13}C^{15}N$ -glutamine (1 mM – Cambridge isotope – product no. CNLM-1275-H) or D_8-arachidonic acid (Cayman – product no. 390010), as previously described.[7,8]

Sample processing and metabolite extraction: A volume of 50µl of frozen RBC aliquots was extracted in 450µl of methanol:acetonitrile:water (5:3:2, *v/v/v*). After vortexing at 4°C for 30 min, extracts were separated from the protein pellet by centrifugation for 10 min at 10,000g at 4°C and stored at −80°C until analysis.

Ultra-High-Pressure Liquid Chromatography-Mass Spectrometry metabolomics: Analyses were performed using a Vanquish UHPLC coupled online to a Q Exactive mass spectrometer (Thermo Fisher, Bremen, Germany). Samples were analyzed using a 3 minute isocratic condition or a 5, 9 and

17 min gradient as described.[9-11] Solvents were supplemented with 0.1% formic acid for positive mode runs and 1 mM ammonium acetate for negative mode runs. MS acquisition, data analysis and elaboration was performed as described. [9-11]

Proteomics Proteomics analyses were performed via FASP digestion and nanoUHPLC-MS/MS identification (nanoEasy LC 1000 coupled to a QExactive HF, Thermo Fisher), as previously described.[12]

Recombinant expression of band 3 N-term peptide 1-56

Unlabeled proteins were grown in Luria broth (LB) while labeled proteins were grown in M9 minimal media (6 g/L Na_2HPO_4, 3 g/L KH_2PO_4, 0.5 g/L NaCl, 1 g/L $^{15}NH_4Cl$, 2 g/L glucose ($^{13}C_6$-glucose if preparing double labeled protein), 2 mL of 1M $MgSO_4$, 100 µL of 1 M $CaCl_2$, 10 mg/L thiamine) unless stated otherwise.

All Band 3 and GAPDH protein constructs contained an N- or C-terminal 6xHis-SUMO. Constructs were cloned into the bacterial expression vector, pET21b, using the NdeI restriction site. Growth media with proper antibiotics was inoculated with a colony from a freshly transformed LB agar plate and shaken at 37 °C for 16 hours. Fresh media was inoculated with 2.5% of the overnight growth and shaken at 37 °C until an OD of 0.6 was reached. Protein expression was induced by the addition of 1 mM isopropyl-beta-D-thiogalactoside (IPTG). Induced cultures were shaken for 4 hours at 37 °C before being harvested by centrifugation at 4,500 rpm for 10 min.

The purification strategy of all protein constructs was similar. Bacterial pellets were resuspended in Lysis Buffer (50 mM Tris pH 7.5, 300 mM NaCl, 3% glycerol, 10 mM imidazole, 10 mM DTT) and lysed by sonication with 7 cycles of 30 sec on, 30 sec off. Cellular debris was removed by centrifugation at 13,000 rpm for 30 min and 4 °C. Lysate was applied to a column packed with Ni Sepharose Excel resin (Cytiva) and washed with 7 column volumes of Lysis Buffer. Bound protein was eluted with 4 column volumes of Elution Buffer (50 mM Tris pH 7.5, 300 mM NaCl, 400 mM imidazole, 5% glycerol). The elution fractions were pooled and SUMO protease (ulp1, in-house) was added. The sample was dialyzed overnight into Lysis Buffer at 4 °C using dialysis tubing with a 3.5K molecular weight cut-off (MWCO). The sample was applied to a column packed with Ni-NTA His•Bind Resin (Sigma) and the flow-through material was collected. The flow-through fraction was concentrated and applied to a Superose 6 Increase column (Cytiva) equilibrated with Storage Buffer (20 mM Bis-Tris pH 6.5, 150 mM NaCl). Fractions containing target protein were pooled, concentrated, and stored at -80 °C.

For the membrane penetrating version of the peptide, three sequences were used based on previous studies:[13,14]

a) Internalization sequence - RQIKIWFQNRRMKWKKGG

b) Poly Arg - CRRRRRRRRC
c) TAT - YGKKRRQRRG

Thermal proteome profiling

Thermal proteome profiling (TPP) were performed as previously described.[15] Lysates from red blood cells were adjusted to 1 mg/mL and divided into 60 aliquotes of 150 µL. Treated lysate samples were incubated with 100 µM Band 3 peptide prior to heating in a thermo cycler (LifeEco, Bioer) at various temperatures (37, 39, 41.5, 44.9, 49.1, 54.1, 58.5, 61.8, 64.7, 67 °C) for 3 min and immediately cooled to 23 °C. Precipitation was removed by centrifugation at 21,000 rcf for 30 min at 4 °C. A 100 µL volume was taken from each sample and reduced and alkylated (4 M Guanidine HCl, 10 mM DTT, 25 mM IAA) for 30 min in the dark. Four volumes of cold acetone were added to the samples and placed at -20 °C overnight to precipitate protein. Precipitated protein was collected by centrifugation at 18,000 rcf, -5 °C for 25 min. Pellets were washed once with cold acetone and residual acetone was removed with use of a SpeedVac (Thermo Fisher Scientific).

Dried pellets were resuspended in 100 µL of digestion buffer (20 mM triethylammonium bicarbonate (TEAB) pH 8.0, 1 µg Lys-C (in-house), 2 µg sequencing grade trypsin (Promega)). Samples were homogenized with the use of a sonicator (Bioruptor Pico, Diagenode) set at 10 °C for twelve cycles of 30 sec on, 30 sec off. Samples were digested overnight at 37 °C with constant mixing at 800 rpm. Samples were isobaric labeled with TMT reagent (TMT10plex, Thermo Fisher) as recommended by the manufacturer. Briefly, TMT reagent dissolved in 100% anhydrous acetonitrile (ACN) was added to the peptide digests at a final ratio of 4:1 (w:w). Samples were incubated at 23 °C for 1 hour with constant mixing at 800 rpm. The reaction was quenched by adding hydroxylamine to a final concentration of 0.5% and incubating at 23 °C for 30 min. TMT labeled samples were combined and dried using a SpeedVac.

Peptide fractionation was performed on a Gemini NX-C18 column (Phenomenex) using a Dionex UltiMate 3000. Peptides were separated using the following gradient: 3% B (0–16.5 min), 3–45% B (16.5–41.5 min), 45–65% B (41.5–46.5 min), 65–100% B (46.5–48.5 min), 100% B (48.5–53.5 min) with solvent A (10 mM ammonium formate, pH 10.0) and solvent B (10 mM ammonium formate, 75% ACN, pH 10.0) at a flow rate of 0.5 mL/min. Fractions were collected every 0.75 minutes and pooled into groups of three. Pooled fractions were dried down with a SpeedVac and acidified with 0.5% formic acid (FA). Acidified peptides were desalted using C18 Spin Tips (Thermo Fisher Scientific) and stored in 0.1% FA at -80 °C for until further analysis.

TMT labeled peptides were analysed by nano-ultrahigh performance (UHP)LC–MS/MS (Easy-nLC1200, Orbitrap Fusion LumosTribrid, Thermo Fisher Scientific). Sample was loaded directly onto an in-house packed 100 µm i.d. × 250 mm fused silica column packed with CORTECS C18 resin (2.7

µm, spherical solid core). Samples were run at 400 nL/min over a 70-min linear gradient from 4 to 32% acetonitrile with 0.1% formic acid. The mass spectrometer was operated in positive ion data-dependent mode. MS1 scans were run in the orbitrap from 375 to 1,500 m/z at 120,000 resolution. Full scan automatic gain control (AGC) and maximum injection time was set to 4 x 10^5 ions and 50 ms. Ions above an intensity threshold of 1 x 10^4 were selected for MS2 analysis with fragmentation by collision induced dissociation (CID). Filtering was performed by the quadrupole with an isolation window of 1.2 m/z. AGC and maximum injection time was set to 1 x 10^4 and 50 ms. Fragmentation was performed by CID with a normalized collision energy of 35%. Detection was set to the ion trap operating in rapid mode. Synchronous precursor selection (SPS) was utilized to co-select 10 MS2 fragments for MS3 analysis. Excluding the precursor, 10 SPS ions were selected within the 400-1200 m/z window. AGC and maximum injection time was set to 1 x 10^5 and 105 ms. The co-selected SPS ions were fragmented by high-energy collisional dissociation (HCD) with a normalized collision energy of 65%, and analyzed in the orbitrap with a resolution of 50,000 and scan range of 100-500 m/z. SPS-MS3 scan frequency was determined by a 3 s total duty cycle.

Proteome Discoverer 2.2 (Thermo Fisher Scientific) was used for the database search and TMT quantification. Raw data was searched against the human Swiss-prot database. Search parameters included carbamidomethylation-C, TMT 10plex-K, and TMT 10plex-peptide N-terminus as fixed modifications, oxidation-M and pyro-Q N-terminus were set as variable modifications. Up to two missed cleavages were allowed with MS1 and MS2 tolerances set to 20 ppm and 0.5 Da. Reporter ion quantification was set at the MS3 level with an integration tolerance of 0.003 Da. A 65% threshold was set for SPS-MS3 mass match.

Melting curve analysis utilized the lowest temperature condition as the reference. Curve fitting and data normalization was performed as previously described.[16] Briefly, the equation

$$f(T) = \frac{1-plateau}{1+e^{-(\frac{a}{T}-b)}} + plateau$$

was used in Prism (GraphPad) for curve fitting and protein T_m determination. The melting point (T_m) is described as the temperature at which the melting curve intercepts 50% protein abundance.

Band 3 Co-IP and chemical cross-linking

Red blood cell lysates were generated by exposing freshly procured and washed RBCs to hypotonic conditions. Lysates were adjusted with IP Buffer (20 mM HEPES pH 7.4, 100 mM NaCl, 1X Halt Protease Inhibitor Cocktail (Thermo Scientific)). The lysates were centrifuged at 18,000 rpm and 4 °C for 20 min to separate the cytosolic and membrane fractions. The membrane fraction was

washed 2 times with IP Buffer. The cytosolic and membrane fractions were diluted to 1 mg/mL with IP Buffer.

Band 3 protein constructs containing either a 6xHis or FLAG tag sequence were used for all co-IP experiments. Cytosolic and membrane fractions were incubated with 50 µM Band 3 protein for 20 min at 4 °C. A second set of samples was prepared for chemical crosslinking with DMTMM and DSSO (disuccinimidyl sulfoxide, Thermo Fisher) followed by co-IP. In brief, DMTMM and DSSO were used at 20 mM and 1 mM, respectively. The reaction was incubated at 23 °C for 30 min before being quenched with the addition of 40 mM ammonium bicarbonate.

Complexes were precipitated by the addition Ni-NTA (88831, Thermo Fisher) or anti-FLAG (A36797, Thermo Fisher) magnetic agarose. The samples were mixed by rotation for 1 hr at 4 °C. The beads were settled in a magnetic tube rack and unbound material was removed by aspiration. Beads were resuspended with IP Buffer and washed by mixing for 10 min. A total of 6 washes were performed. Bound protein was eluted in 2 rounds with the addition of FLAG peptide (A6002, APExBIO Technology) or 400 mM imidiazole.

The eluted protein was proteolytically digested according to the FASP protocol as previously described[17]. In brief, 300 µg of each sample was reduced, alkylated, and digested at 1:50 with sequencing grade trypsin and mass spectrometry grade rAsp-N (Promega) by incubating at 37 °C for 18 h. Peptides were eluted and acidified to 0.1% formic acid. Crosslinked co-IP samples received an addition enrichment step of strong cation exchange chromatography (SCX) with a Dionex UltiMate 3000 system (Thermo Fisher Scientific). A Proteomix SCX-NP1.7 column (4.6 mm inner diameter, 150 mm length, Sepax Technologies) was used. In brief, peptides were separated using the following gradient: 0% B (0–3.5 min), 0–22.5% B (3.5–18.5 min), 22.5–50% B (18.5–21.5 min), 50–100% B (21.5–23 min), 100% B (23–25.5 min) with solvent A (10 mM KH2PO4, 25% acetonitrile, pH 3.00) and solvent B (10 mM KH2PO4, 25% acetonitrile, 500 mM KCl, pH 3.00) at a flow rate of 0.7 ml/min. Fractions were collected every minute. Fractions 6–26 were pooled into groups of three. All samples were desalted using Pierce C18 Spin Tips (Thermo Fisher Scientific) for subsequent liquid chromatography with tandem mass spectrometry (LC–MS/MS) analysis.

All samples were analysed by nano-ultrahigh performance (UHP)LC–MS/MS (Easy-nLC1200, Orbitrap Fusion LumosTribrid, Thermo Fisher Scientific). Sample was loaded directly onto an in-house packed 100 µm i.d. × 250 mm fused silica column packed with CORTECS C18 resin (2.7 µm, spherical solid core) and run at 400 nL/min over a 70-min gradient from 4 to 32% acetonitrile with 0.1% formic acid. Non-crosslinked and DMTMM treated samples used a MS2 acquisition method. In brief, MS1 scans were run in the orbitrap from 300 to 1,600 m/z at 120,000 resolution. MS2 was performed in a stoichiometric fashion on top ions from each precursor scan and fragmented

at a HCD collision energy of 30%. MS2 scan frequency was determined by a 5 s total duty cycle. DSSO treated samples utilized an MS3 acquisition scheme. DSSO treated samples were analyzed as previously described.[18] In brief, MS1 scans were run in the orbitrap from 375 to 1,500 m/z at 60,000 resolution. MS2 was performed in a stoichiometric fashion on top ions from each precursor scan and fragmented at a CID collision energy of 22%. MS2 scan frequency was determined by a 5-s total duty cycle. MS3 was triggered by the targeted mass difference of 31.9721 Da, and was performed as a stepped HCD collision energy of 33 ± 3%. Data acquisition was performed using Xcalibur (version 4.1) software.

Instrument data from the non-crosslinked and DSSO treated samples were directly loaded in to Proteome Discoverer 2.2 and searched against the human Swiss-prot database. Constant search parameters included carbamidomethylation-C as a fixed modification, oxidation-M, and pyro-Q N-terminus as variable modifications, allowing for two missed cleavages. DSSO related variable modifications, DSSO-K, DSSO/amidated-K, and DSSO/hydrolysed-K were added for DSSO specific searches. Precursor mass tolerance was set to 10 p.p.m., with MS/MS mass tolerance set to 20 p.p.m. The XlinkX node was used for DSSO crosslink searches and MS2_MS3 was set for crosslink detection. Results were visualized using xiVIEW.[19] Instrument raw files from DMTMM treated samples were directly loaded into MetaMorpheus and searched using the MetaMorpheusXL task.[20] Search parameters included carbamidomethylation-C as a fixed modification, oxidation-M and pyro-Q N-terminus as variable modifications, allowing for two missed cleavages. DMTMM was added as a selectable crosslinker. Precursor mass tolerance was set to 10 p.p.m., with MS/MS mass tolerance set to 20 p.p.m. Results were visualized using xiVIEW.[19]

Cross-linking proteomics Protein complexes consisting of GAPDH and band 3 truncations were crosslinked with 20 mM DMTMM (4-(4,6-dimethoxy-1,3,5-triazin-2-yl)-4-methyl-morpholinium chloride, Sigma) for 1 hr at room temperature. The reaction was quenched by the addition of ammonium bicarbonate to a final concentration of 50 mM. The crosslinked complex was proteolytically digested according to the FASP (filter-aided sample preparation) protocol as previously described[17]. In brief, ~200 µg of crosslinked sample was reduced, alkylated, and digested at 1:50 with sequencing grade trypsin and mass spectrometry grade rAsp-N (Promega) by incubating at 37 °C for 18 h. Peptides were eluted and acidified to 0.1% formic acid. Enrichment of crosslinked peptides was performed by using strong cation exchange chromatography (SCX) with a Dionex UltiMate 3000 system (Thermo Fisher Scientific). A Proteomix SCX-NP1.7 column (4.6 mm inner diameter, 150 mm length, Sepax Technologies) was used. In brief, peptides were separated using the following gradient: 0% B (0–3.5 min), 0–22.5% B (3.5–18.5 min), 22.5–50% B (18.5–21.5 min), 50–

100% B (21.5–23 min), 100% B (23–25.5 min) with solvent A (10 mM KH2PO4, 25% acetonitrile, pH 3.00) and solvent B (10 mM KH2PO4, 25% acetonitrile, 500 mM KCl, pH 3.00) at a flow rate of 0.7 ml/min. Fractions were collected every minute. Fractions 6–26 were pooled into groups of three and desalted using Pierce C18 Spin Tips (Thermo Fisher Scientific) for subsequent liquid chromatography with tandem mass spectrometry (LC–MS/MS) analysis. Crosslinked peptides were analysed by nano-ultrahigh performance (UHP)LC–MS/MS (Easy-nLC1200, Orbitrap Fusion LumosTribrid, Thermo Fisher Scientific). Sample was loaded directly onto an in-house packed 100 µm i.d. × 250 mm fused silica column packed with CORTECS C18 resin (2.7 µm, spherical solid core). Samples were run at 400 nl/min over a 70-min linear gradient from 4 to 32% acetonitrile with 0.1% formic acid. The mass spectrometer was operated in positive ion mode. MS1 scans were run in the orbitrap from 300 to 1,600 m/z at 120,000 resolution. MS2 was performed in a stoichiometric fashion on top ions from each precursor scan and fragmented at a HCD collision energy of 30%. MS2 scan frequency was determined by a 5 s total duty cycle. Data acquisition was performed using Xcalibur (version 4.1) software. Instrument raw files were loaded into MetaMorpheus and searched using the MetaMorpheusXL task.[20] Search parameters included carbamidomethylation-C as a fixed modification and oxidation-M as variable modifications, allowing for two missed cleavages. DMTMM was added as a selectable crosslinker type (-H2O, -18.01056 Da). Residue specificity of DMTMM crosslinks was considered as the following: position 1 to position 2, where position 1 is either the protein N-terminus or Lys and position 2 is either the protein C-terminus, Asp, or Glu. Precursor mass tolerance was set to 10 p.p.m., with MS/MS mass tolerance set to 20 ppm. Results were visualized using xiVIEW[19] and Proxl.[21]

Isothermal Titration calorimetry (ITC) All ITC binding experiments were performed with a MicroCal iTC_{200} (Cytiva) set at 25 °C. GAPDH and Band 3 proteins were dialyzed into matching buffer (20 mM Bis-Tris pH 6.5, 50 mM NaCl, 2 mM DTT). The cell contained GAPDH at 0.1 mM while the syringe contained Band 3 at 1 mM. Reference power was set to 10 µcal/sec with a constant stirring speed of 1000 rpm. A total of 20 injections were performed. The first injection was excluded from data analysis. Experiments were performed in duplicate and the results were analyzed with the Origin ITC module.

Nuclear Magnetic Resonance and structural models ^{15}N-heteronuclear single quantum coherence (HSQC) spectra were collected at 25ºC for the recombinantly expressed band 3 peptide 1-56 in the presence of 100 and 200 uM GAPDH. Data were collected on a Varian 900 using a standard ^{15}N-HSQC sequence.

Statistical Analyses: Graphs and statistical analyses (either T-test or repeated measures ANOVA) were prepared with GraphPad Prism 5.0 (GraphPad Software, Inc, La Jolla, CA) and MetaboAnalyst 4.0.[22]

SUPPLEMENTARY RESULTS AND DISCUSSION ON THE RBC INTERACTOME

The Red Blood Cell Interactome as gleaned by cross-linking proteomics

The human body contains 25 trillion red blood cells (RBCs - 83% of all human cells)[23,24] Each erythrocyte contains ~250-270 million molecules of hemoglobin and allows the transport of up to 1 billion molecules of oxygen/cell[23,24]. These numbers also explain why hemoglobin makes up for ~92% of the total protein content in a mature RBC.[25] To maximize intracellular hemoglobin content, erythroid precursors progressively lose nuclei and organelles during maturation to RBC.[26]

Another unique characteristic of non-nucleated RBCs is that the plasma membrane, its only structural component, and membrane proteins account for all of its diverse antigenic, transport, and mechanical characteristics.[27] Over the decades, careful biochemical studies have elucidated the relevance of membrane protein interactions in the regulation of the RBC cytoskeletal properties, which allow the stabilization of the erythrocyte membrane during RBC turbulent flow from the lungs into the capillary beds as small as 3 μm.[1] Based on biochemical data and imaging approaches,[28] biophysical models of RBC membrane structure and function have been generated that allow to simulate RBC responses to energy-induced cytoskeletal defects,[29] as well as mechanical and osmotic stress.[30]

Despite the apparent simplicity, advancements in the field of mass spectrometry-based proteomics have catalogued over 2000 proteins in highly-purified erythrocytes,[31] which are closer to ~3000 protein entries when reports from multiple studies are merged.[12,32-34] Based on these lists, *in silico* approaches have tried to predict protein-protein interactions[35,36] – the interactome – in an attempt to update our understanding of RBC physiology. To follow up on these predictions, biochemical approaches were devised to investigate protein-protein interactions in the form of multimeric complexes by means of native gel electrophoresis studies.[37] Unfortunately, these techniques were affected by slow throughputness and lack of precision in the identification of such complexes, other than validation of actual direct interaction based on close structural proximity of protein components of the putatively assigned complexes.

To overcome these limitations, in the present study we adopted a novel cross-linking proteomics approach, based on multiple cross-linking agents. This strategy, coupled to high-resolution MS^3 mass spectrometry, allows to chemically stabilize protein-protein interactions by bridging epsilon amine residues of K residues and carboxylic groups in the side chains of acidic amino acids D and E, provided they face each other within a given range (e.g., 11.4 to 24 Å for the zero-length cross-linking agents we used in this study).[18,20,38] Through this approach we mapped over 5597

peptide-peptide unique inter- or intra-molecular cross-links, involving a total of 134 unique RBC proteins, generating a preliminary map of the RBC experimental interactome.

Red Blood Cell experimental interactome as gleaned by cross-linking proteomics experiments

RBC cytosols and membranes were incubated with two different cross-linking agents, DSSO and DMTMM. This approach affords determination of protein-protein interactions by cross-linking free epsilon-amines of adjacent residues of interacting proteins between each other (DSSO-**Supplementary Figure 6.A**) or carboxylic group of D/E residues (DMTMM) within a range spanning from 11.4 to 24 Å.[18,38] Cross-linked proteins were thus enzymatically digested with trypsin, which cleave at the C-term of basic K or R residues, prior to high-pH reversed phase fractionation to enrich for cross-linked peptides owing to their positive charge as a result of tryptic cleavage at basic residues on both peptides (**Supplementary Figure 6.B**). Results are extensively reported in tabulated form in **Supplementary Table 1** – including a list of 5597 unique peptide-peptide cross-links, their sequence, protein identification (Uniprot ID), positions of the cross-link on the peptide and whole protein sequence. Additionally, we report the fraction (cytoslic vs membrane) and the specific cross-link (DSSO or DMTMM) that enabled the identification of the interacting peptides.

To facilitate the visualization of the experimentally identified protein-protein interactions, we plotted our results in the form of circos plots (**Supplementary Figure 6.C**) and network views (**Supplementary Figure 6.D**). In both cases, proteins are connected by a line (edge) whenever experimental interactions were assigned. The proteins with the highest number of experimental interactions (highest degree) will map at the center of the network. In this view, it is worth highlighting that hemoglobin chains (HBB and HBA) where characterized by the highest number of potential interactors – which was expected owing to the elevated intracellular hemoglobin content and the proportionally increased likelihood of K or D/E residues on hemoglobin to face K or D/E residues on other RBC proteins within 11-24 Å range, by sheer molecular crowding. However, this analysis also highlighted a core of highly-interacting proteins, mostly structural components, including the anion exchanger band 3 (B3AT), ankyrin (ANK1), spectrin alpha and beta (SPTA1 and SPTB1 – **Supplementary Figure 6.D**).

Cross-linking proteomics studies recapitulate structural elucidation of hemoglobin tetramers

One of the advantages of the cross-linking proteomics approach is that it not only highlights the intermolecular interactions between two distinct proteins, but also affords resolution of intramolecular interactions whenever basic and acidic residues that are substrates for the cross-linker face each other within the same protein/protein complex in the linker range. This approach is thus useful to refine

knowledge on the structure of molecular complexes, which may be relevant in case the structure or oligomeric conformation of a molecule are unknown. Vice versa, since this is the first report adopting this method in RBCs, we decided to test the reliability of our findings against protein structures that are extremely well-established. The paradigmatic example of the statement above is hemoglobin.

First of all, we graphed intra- (purple lines) and inter-molecular interactions (teal) between hemoglobin chains alpha and beta - HBA and HBB as bar plots (**Supplementary Figure 7.A**). We then mapped these interaction against the crystal structure of the human oxyhemoglobin tetramer (the present experiments were performed under atmospheric oxygen) solved by Terrell et al. (pdb: 6BB5 – **Supplementary Figure 7.B**). As proof of principle, we highlighted the experimentally identified interacting residues for K18 of HBA and their distance to neighboring residues (**Supplementary Figure 7.C**). In addition, in **Supplementary Figure 7.D** we show a representative mass spectrum from MS3 analyses of one of the highest-scores cross-links, between the peptides containing K12 and E122 of HBA and HBB, respectively (y and b series ions are annotated). Finally, in **Supplementary Figure 7.E**-**F**, we show the matrix plots for the experimentally identified cross-links between HBA and HBB (teal) or within HBB (purple for intra and teal for inter-chain cross-links).

Experimental interactome of red blood cell membrane proteins

The RBC membrane interactome is a critical lynchpin for the erythrocyte cytoskeleton. The dynamic nature of membrane protein interaction is also critical to RBC capacity to respond to shear and mechanical stress when traversing narrow capillaries in the peripheral vasculature.[28] Integral membrane protein components not only participate in anchoring the membrane to the cytoskeleton, but also contribute to blood groups and other RBC membrane immunomodulators/antigens that impact untimely removal from the bloodstream, such as B3AT oligomeric state.[39] As such, RBC membrane protein interactions have represented one of the early focuses of structural biologist when tackling erythrocyte complexity.[40-43] By focusing on the membrane fraction of RBC lysates, we managed to overcome some of the limitations noted above with respect to the overwhelming abundance of hemoglobin. This approach allowed us to map the intra- and intermolecular interactome of RBC structural protein components, to expand upon existing literature. Caveats in the interpretation of the present results is that the experimental findings reported here are not meant to overwrite decades of careful biochemistry focused on isolated protein components, rather to complement such information based on evidence generated with a brand new tool that affords mapping of many more such intra and inter-molecular interactions in a single experiment.

Specifically, in **Supplementary Figure 8.A** we highlighted a network of RBC membrane proteins according to the canonical models[27] (proteins are abbreviated as Uniprot gene names). Zooming in

from the network view, in **Supplementary Figure 8.B** we provide an overview of the interactions across these proteins in bar plot format. The complexity of this network is apparent when expanding the bar plots to focus on band 3 (B3AT), spectrin alpha and beta (SPTA1 and SPTB1), ankyrins 1 and 2 (ANK1 and ANK2), carbonic anhydrase 1 and 2 (CAH1 and CAH2), erythrocyte protein band 4.1 and 4.2 (41 and EPB42 - **Supplementary Figure 8.C**). Further zooming in on the B3AT cytosolic and extracellular domains, we highlighted the intramolecular interaction of band 3 (residues 56-356 – *1HYN.pdb*[44] and 381-886 – *4YZF.pdb*[45], **Supplementary Figure 8.D** and **E**, respectively).

On top of the well-established networks involving the membrane protein components above, in this study we also identified a sub-network of structural proteins interacting with SPTB1 (**Supplementary Figure 8.F**), including tropomodulin 1 (TMOD1), cytoplasmic actin (ACTG), and the glycolytic enzyme triosephosphate isomerase (TPIS), other than intramolecular cross-links in SPTB1 itself (*1S35.pdb*[46] – **Supplementary Figure 8.G-H**).

Cross-linking proteomics evidence of the interactions between the N-terminus of band 3 and hemoglobin or glycolytic enzymes

The interactome of RBC membrane proteins has been suggested to play functional role in erythrocyte physiology beyond cytsokeletal homeostasis. One paradigmatic example of such interaction is found in the N-terminus cytosolic domain of B3AT. The two most abundant cytosolic and membrane proteins in RBCs – hemoglobin and B3AT, have long been shown to interact[47,48] Hemoglobin, especially under deoxygenated conditions, has been shown to outcompete glycolytic enzymes, among which glyceraldehyde 3-phosphate dehydrogenase (GAPDH – **Figure 6**), which are otherwise bound to the N-term of B3AT and inhibited. Through this mechanism, RBCs regulate metabolic fluxes through glycolysis and the pentose phosphate pathway to generate energy or reducing equivalents to counteract oxidant stress in response to hypoxia or high oxygen saturation-induced oxidant stress, respectively[1,49].

Hemoglobin and glycolytic enzyme interactions to B3AT are now supported by a plethora of data, based on immunological assays (co-immunoprecipitation, western blot on everted membranes, immunofluorescence), enzymatic activity assays, determination of metabolic fluxes via nuclear magnetic resonance and mass spectrometry-based metabolic flux analysis as determined via stable-isotope labeled tracers.[50-56] Such interactions were further determined mechanistically by studies in mice carrying genetic ablation of specific sequences (residues 1-11 and 12-23) of B3AT.[1,49] However, the actual structural underpinning of B3AT binding to hemoglobin or glycolytic enzymes is difficult to investigate experimentally through classic structural approaches such as nuclear magnetic resonance, owing to the dynamic conformational changes of the B3AT N-terminus. Indeed, while the

structure of the N-terminus of AE1 beyond residue K56 has been solved through crystallography[44], the very first residues 1-56 of the N-terminus B3AT arrange into an intrinsically disorder domain that has hitherto eluded structural studies. Besides, structural studies aimed at determining B3AT N-term structural interactions has so far eluded also early proteomics studies reliant on cross-linking agents and previous generation mass spectrometers.[50] In addition, the B3AT N-terminus is extremely acidic and the first trypsin cleavable residue (K56) generates a very long peptide that often times eludes detection at the mass spectrometry level. In the present study we overcame those limitations by combining multiple as multiple cross-linking agents (DSSO and DMTMM) to capture this interaction, as well as multiple enzyme digestion strategies (trypsin and Asp-N) followed by enrichment of B3AT-hemoglobin cross-links, which were then identified by new generation high-resolution MS3 analysis and mapped as bar plot in **Supplementary Figure 9.A**. Specifically, most interactions between B3AT and hemoglobin chains (especially HBB – **Supplementary Figure 9.B**) mapped on residues 1-56 and 150-210 of B3AT (**Supplementary Figure 9.A-B**). In **Supplementary Figure 9.C** and **D**, these interactions are mapped against hemoglobin structure and B3AT cytosolic regions 1-15 (*2BTA.pdb*[57]) and 56-356.

Discussion

Mapping RBC protein-protein interactions has critical implications for expanding our understanding of RBC physiology in health and disease. Being devoid of de novo protein synthesis capacity, to quickly respond to environmental stimuli, RBCs rely on post-translational modifications (e.g., phosphorylation) and the impact these have on protein-protein interactions and protein function.[42,58] Competitive interactions between hemoglobin and glycolytic enzymes with the N-terminus of band 3 have been investigated over the years as a critical pathway in response to environmental oxygen tension and oxidant stress.[42,50,52,59-62] Interactions between the band 3-spectrin-ankyrin cytoskeleton, along with actin, adducin and protein 4.1 have been extensively described as key regulators of RBC membrane stability and deformability in the classic model of the RBC cytoskeleton.[27] On top of intermolecular interactions, changes in the multimeric state of RBC structural proteins may have immunogenic potential, such as in the case of band 3 oligomerization triggering RBC recognition by naturally occurring antibodies[63] and subsequent removal from the bloodstream.

Advances in the field of proteomics have revealed the unanticipated complexity of the RBC proteome,[12,31-34] and informed in silico studies to predict how these proteins may interact in a way that could impact RBC physiology.[35,36] Here we leveraged a novel cross-linking proteomics approach to provide the first map of the experimental cytosolic and membrane RBC interactome. To validate

some of our key findings, we mapped the experimentally-identified intramolecular interactions against available protein structures for the hemoglobin tetramer. We thus focus on the RBC membrane interactome, with an emphasis on band 3 and its interactions with structural components, hemoglobin and glycolytic enzymes.

This study holds several limitations. First of all, in this proof of principle study we used hemoglobin intra- and inter-molecular interactions as an internal validation for the reliability of the approach. However, the overwhelming abundance of hemoglobin, despite the high pH-RP fractionation approach aimed at enriching cross-linked peptides, has hampered the detection of other cross-links involving low abundance protein components – limiting the depth of the analysis. In addition, the abundance of hemoglobin may have favored the identification of spurious cross-links, simply by stochastically increasing the likelihood of solvent accessible K or D/E residues on hemoglobin to be exposed to other cross-linkable residues on other proteins. These sub-stoichiometric events either eluded detection at the mass spectrometry level, their signal covered by more abundant hits, or resulted in low score events that were filtered out upon curation of the data in **Supplementary Table 1**.

Despite these limitations, the study offers a proof-of-principle of the applicability of this method to investigate changes to the RBC interactome in health and disease. For example, in a classic review, Mohandas and Gallagher report that 1 in 6 humans in the world, more than 1 billion people, are affected by RBC abnormalities owing to the natural selection driven by malaria, making them the most common of the inherited disorders.[27] Abnormalities at the enzymatic level, such as deficient glucose 6-phosphate dehydrogenase activity, affect ~400 million people and have bene reported to impact RBC morphology and storage quality.[4,64] RBC structural defects impacting structural/functional protein components, from sickle cell disease to hereditary spherocytosis, from rare conditions impacting one of the key lynchpin of our interactome from the present study, the N-terminus of band 3, as in the case of band 3 *Neapolis*.[3] Similarly, recent studies have highlighted how viral infections, including SARS-CoV-2, may impact RBC membrane structural integrity by triggering fragmentation of structural components such as the cytosolic domain of band 3.[65]

Supplementary References

1. Chu H, McKenna MM, Krump NA, et al. Reversible binding of hemoglobin to band 3 constitutes the molecular switch that mediates O2 regulation of erythrocyte properties. *Blood*. 2016;128(23):2708-2716.
2. Howie HL, Hay AM, de Wolski K, et al. Differences in Steap3 expression are a mechanism of genetic variation of RBC storage and oxidative damage in mice. *Blood Adv*. 2019;3(15):2272-2285.
3. Perrotta S, Borriello A, Scaloni A, et al. The N-terminal 11 amino acids of human erythrocyte band 3 are critical for aldolase binding and protein phosphorylation: implications for band 3 function. *Blood*. 2005;106(13):4359-4366.
4. Francis RO, D'Alessandro A, Eisenberger A, et al. Donor glucose-6-phosphate dehydrogenase deficiency decreases blood quality for transfusion. *J Clin Invest*. 2020;130(5):2270-2285.
5. de Wolski K, Fu X, Dumont LJ, et al. Metabolic pathways that correlate with post-transfusion circulation of stored murine red blood cells. *Haematologica*. 2016;101(5):578-586.
6. Reisz JA, Wither MJ, Dzieciatkowska M, et al. Oxidative modifications of glyceraldehyde 3-phosphate dehydrogenase regulate metabolic reprogramming of stored red blood cells. *Blood*. 2016;128(12):e32-42.
7. Reisz JA, Nemkov T, Dzieciatkowska M, et al. Methylation of protein aspartates and deamidated asparagines as a function of blood bank storage and oxidative stress in human red blood cells. *Transfusion*. 2018.
8. Nemkov T, Sun K, Reisz JA, et al. Metabolism of Citrate and Other Carboxylic Acids in Erythrocytes As a Function of Oxygen Saturation and Refrigerated Storage. *Front Med (Lausanne)*. 2017;4:175.
9. Nemkov T, Hansen KC, D'Alessandro A. A three-minute method for high-throughput quantitative metabolomics and quantitative tracing experiments of central carbon and nitrogen pathways. *Rapid Commun Mass Spectrom*. 2017;31(8):663-673.
10. Nemkov T, Reisz JA, Gehrke S, Hansen KC, D'Alessandro A. High-Throughput Metabolomics: Isocratic and Gradient Mass Spectrometry-Based Methods. *Methods Mol Biol*. 2019;1978:13-26.
11. Reisz JA, Zheng C, D'Alessandro A, Nemkov T. Untargeted and Semi-targeted Lipid Analysis of Biological Samples Using Mass Spectrometry-Based Metabolomics. *Methods Mol Biol*. 2019;1978:121-135.
12. D'Alessandro A, Dzieciatkowska M, Nemkov T, Hansen KC. Red blood cell proteomics update: is there more to discover? *Blood Transfus*. 2017;15(2):182-187.
13. Kalafatovic D, Giralt E. Cell-Penetrating Peptides: Design Strategies beyond Primary Structure and Amphipathicity. *Molecules*. 2017;22(11).
14. Bechara C, Sagan S. Cell-penetrating peptides: 20 years later, where do we stand? *FEBS Lett*. 2013;587(12):1693-1702.
15. Franken H, Mathieson T, Childs D, et al. Thermal proteome profiling for unbiased identification of direct and indirect drug targets using multiplexed quantitative mass spectrometry. *Nat Protoc*. 2015;10(10):1567-1593.
16. Savitski MM, Reinhard FB, Franken H, et al. Tracking cancer drugs in living cells by thermal profiling of the proteome. *Science*. 2014;346(6205):1255784.
17. Wisniewski JR, Zougman A, Nagaraj N, Mann M. Universal sample preparation method for proteome analysis. *Nat Methods*. 2009;6(5):359-362.
18. Li X, Liu S, Zhang L, et al. A unified mechanism for intron and exon definition and back-splicing. *Nature*. 2019;573(7774):375-380.
19. Graham M, Combe C, Kolbowski L, Rappsilber J. xiView: A common platform for the downstream analysis of Crosslinking Mass Spectrometry data. *bioRxiv*. 2019:561829.
20. Lu L, Millikin RJ, Solntsev SK, et al. Identification of MS-Cleavable and Noncleavable Chemically Cross-Linked Peptides with MetaMorpheus. *J Proteome Res*. 2018;17(7):2370-2376.
21. Riffle M, Jaschob D, Zelter A, Davis TN. ProXL (Protein Cross-Linking Database): A Platform for Analysis, Visualization, and Sharing of Protein Cross-Linking Mass Spectrometry Data. *J Proteome Res*. 2016;15(8):2863-2870.
22. Chong J, Soufan O, Li C, et al. MetaboAnalyst 4.0: towards more transparent and integrative metabolomics analysis. *Nucleic Acids Res*. 2018;46(W1):W486-W494.

23. Bianconi E, Piovesan A, Facchin F, et al. An estimation of the number of cells in the human body. *Ann Hum Biol*. 2013;40(6):463-471.
24. Sender R, Fuchs S, Milo R. Revised Estimates for the Number of Human and Bacteria Cells in the Body. *PLoS Biol*. 2016;14(8):e1002533.
25. Nemkov T, Reisz JA, Xia Y, Zimring JC, D'Alessandro A. Red blood cells as an organ? How deep omics characterization of the most abundant cell in the human body highlights other systemic metabolic functions beyond oxygen transport. *Expert Rev Proteomics*. 2018;15(11):855-864.
26. Palis J. Primitive and definitive erythropoiesis in mammals. *Front Physiol*. 2014;5:3.
27. Mohandas N, Gallagher PG. Red cell membrane: past, present, and future. *Blood*. 2008;112(10):3939-3948.
28. Nans A, Mohandas N, Stokes DL. Native ultrastructure of the red cell cytoskeleton by cryo-electron tomography. *Biophys J*. 2011;101(10):2341-2350.
29. Gov NS, Safran SA. Red blood cell membrane fluctuations and shape controlled by ATP-induced cytoskeletal defects. *Biophys J*. 2005;88(3):1859-1874.
30. Fedosov DA, Caswell B, Karniadakis GE. A multiscale red blood cell model with accurate mechanics, rheology, and dynamics. *Biophys J*. 2010;98(10):2215-2225.
31. Gautier EF, Leduc M, Cochet S, et al. Absolute proteome quantification of highly purified populations of circulating reticulocytes and mature erythrocytes. *Blood Adv*. 2018;2(20):2646-2657.
32. Bryk AH, Wisniewski JR. Quantitative Analysis of Human Red Blood Cell Proteome. *J Proteome Res*. 2017;16(8):2752-2761.
33. Pasini EM, Kirkegaard M, Salerno D, Mortensen P, Mann M, Thomas AW. Deep coverage mouse red blood cell proteome: a first comparison with the human red blood cell. *Mol Cell Proteomics*. 2008;7(7):1317-1330.
34. Wilson MC, Trakarnsanga K, Heesom KJ, et al. Comparison of the Proteome of Adult and Cord Erythroid Cells, and Changes in the Proteome Following Reticulocyte Maturation. *Mol Cell Proteomics*. 2016;15(6):1938-1946.
35. D'Alessandro A, Righetti PG, Zolla L. The red blood cell proteome and interactome: an update. *J Proteome Res*. 2010;9(1):144-163.
36. Goodman SR, Kurdia A, Ammann L, Kakhniashvili D, Daescu O. The human red blood cell proteome and interactome. *Exp Biol Med (Maywood)*. 2007;232(11):1391-1408.
37. Pallotta V, D'Alessandro A, Rinalducci S, Zolla L. Native protein complexes in the cytoplasm of red blood cells. *J Proteome Res*. 2013;12(7):3529-3546.
38. Schmitt LR, Henderson R, Barrett A, et al. Mass spectrometry-based molecular mapping of native FXIIIa cross-links in insoluble fibrin clots. *J Biol Chem*. 2019;294(22):8773-8778.
39. Karon BS, Hoyer JD, Stubbs JR, Thomas DD. Changes in Band 3 oligomeric state precede cell membrane phospholipid loss during blood bank storage of red blood cells. *Transfusion*. 2009;49(7):1435-1442.
40. Bruce LJ, Beckmann R, Ribeiro ML, et al. A band 3-based macrocomplex of integral and peripheral proteins in the RBC membrane. *Blood*. 2003;101(10):4180-4188.
41. Dahl KN, Parthasarathy R, Westhoff CM, Layton DM, Discher DE. Protein 4.2 is critical to CD47-membrane skeleton attachment in human red cells. *Blood*. 2004;103(3):1131-1136.
42. Ferru E, Giger K, Pantaleo A, et al. Regulation of membrane-cytoskeletal interactions by tyrosine phosphorylation of erythrocyte band 3. *Blood*. 2011;117(22):5998-6006.
43. Kalli AC, Reithmeier RAF. Interaction of the human erythrocyte Band 3 anion exchanger 1 (AE1, SLC4A1) with lipids and glycophorin A: Molecular organization of the Wright (Wr) blood group antigen. *PLoS Comput Biol*. 2018;14(7):e1006284.
44. Zhang D, Kiyatkin A, Bolin JT, Low PS. Crystallographic structure and functional interpretation of the cytoplasmic domain of erythrocyte membrane band 3. *Blood*. 2000;96(9):2925-2933.
45. Arakawa T, Kobayashi-Yurugi T, Alguel Y, et al. Crystal structure of the anion exchanger domain of human erythrocyte band 3. *Science*. 2015;350(6261):680-684.
46. Kusunoki H, MacDonald RI, Mondragon A. Structural insights into the stability and flexibility of unusual erythroid spectrin repeats. *Structure*. 2004;12(4):645-656.

47. Chu H, Breite A, Ciraolo P, Franco RS, Low PS. Characterization of the deoxyhemoglobin binding site on human erythrocyte band 3: implications for O2 regulation of erythrocyte properties. *Blood*. 2008;111(2):932-938.
48. Sega MF, Chu H, Christian J, Low PS. Interaction of deoxyhemoglobin with the cytoplasmic domain of murine erythrocyte band 3. *Biochemistry*. 2012;51(15):3264-3272.
49. Chu H, Low PS. Mapping of glycolytic enzyme-binding sites on human erythrocyte band 3. *Biochem J*. 2006;400(1):143-151.
50. Puchulu-Campanella E, Chu H, Anstee DJ, Galan JA, Tao WA, Low PS. Identification of the components of a glycolytic enzyme metabolon on the human red blood cell membrane. *J Biol Chem*. 2013;288(2):848-858.
51. Sun K, Zhang Y, D'Alessandro A, et al. Sphingosine-1-phosphate promotes erythrocyte glycolysis and oxygen release for adaptation to high-altitude hypoxia. *Nat Commun*. 2016;7:12086.
52. Lewis IA, Campanella ME, Markley JL, Low PS. Role of band 3 in regulating metabolic flux of red blood cells. *Proc Natl Acad Sci U S A*. 2009;106(44):18515-18520.
53. von Ruckmann B, Schubert D. The complex of band 3 protein of the human erythrocyte membrane and glyceraldehyde-3-phosphate dehydrogenase: stoichiometry and competition by aldolase. *Biochim Biophys Acta*. 2002;1559(1):43-55.
54. Eisenmesser EZ, Post CB. Insights into tyrosine phosphorylation control of protein-protein association from the NMR structure of a band 3 peptide inhibitor bound to glyceraldehyde-3-phosphate dehydrogenase. *Biochemistry*. 1998;37(3):867-877.
55. Liu H, Zhang Y, Wu H, et al. Beneficial Role of Erythrocyte Adenosine A2B Receptor-Mediated AMP-Activated Protein Kinase Activation in High-Altitude Hypoxia. *Circulation*. 2016;134(5):405-421.
56. Rogers SC, Said A, Corcuera D, McLaughlin D, Kell P, Doctor A. Hypoxia limits antioxidant capacity in red blood cells by altering glycolytic pathway dominance. *FASEB J*. 2009;23(9):3159-3170.
57. Schneider ML, Post CB. Solution structure of a band 3 peptide inhibitor bound to aldolase: a proposed mechanism for regulating binding by tyrosine phosphorylation. *Biochemistry*. 1995;34(51):16574-16584.
58. Azouzi S, Romana M, Arashiki N, et al. Band 3 phosphorylation induces irreversible alterations of stored red blood cells. *Am J Hematol*. 2018;93(5):E110-E112.
59. Castagnola M, Messana I, Sanna MT, Giardina B. Oxygen-linked modulation of erythrocyte metabolism: state of the art. *Blood Transfus*. 2010;8 Suppl 3:s53-58.
60. Messana I, Ferroni L, Misiti F, et al. Blood bank conditions and RBCs: the progressive loss of metabolic modulation. *Transfusion*. 2000;40(3):353-360.
61. Messana I, Orlando M, Cassiano L, et al. Human erythrocyte metabolism is modulated by the O2-linked transition of hemoglobin. *FEBS Lett*. 1996;390(1):25-28.
62. Stefanovic M, Puchulu-Campanella E, Kodippili G, Low PS. Oxygen regulates the band 3-ankyrin bridge in the human erythrocyte membrane. *Biochem J*. 2013;449(1):143-150.
63. Pantaleo A, Giribaldi G, Mannu F, Arese P, Turrini F. Naturally occurring anti-band 3 antibodies and red blood cell removal under physiological and pathological conditions. *Autoimmun Rev*. 2008;7(6):457-462.
64. D'Alessandro A, Fu X, Kanias T, et al. Donor sex, age and ethnicity impact stored red blood cell antioxidant metabolism through mechanisms in part explained by glucose 6-phosphate dehydrogenase levels and activity. *Haematologica*. 2020.
65. Thomas T, Stefanoni D, Dzieciatkowska M, et al. Evidence of Structural Protein Damage and Membrane Lipid Remodeling in Red Blood Cells from COVID-19 Patients. *J Proteome Res*. 2020;19(11):4455-4469.

Supplementary Table 1

	Patient	N.V.
Red Blood Cells (10^6/µL)	3.47	4.2-5.5
Hemoglobin (g/dL)	11.3	12-18
Hematocrit (%)	36.7	37-52
Mean Corpuscolar Value (fL)	105.8	80-99
Mean Corpuscular Hemoglobin (pg)	32.6	26-31
Mean Corpuscular Hemoglobin Concentration (g/dL)	30.8	31-36
Red Blood Cell Distribution Width – SD (fL)	90	38-44
Red Blood Cell Distribution Width – CV (%)	24.5	11-15
Platelets (10^3/ µL)	659	150-450
Reticulocytes (10^6/µL)	0.35	0.02-0.1
Total Bilirubin (mg/dL)	10.96	<1.2
Indirect bilirubin (mg/dL)	10.41	<0.8
Lactate dehydrogenase (U/L)	867	120-240
Ferritin (ng/mL)	103	20-400

Supplementary Figures

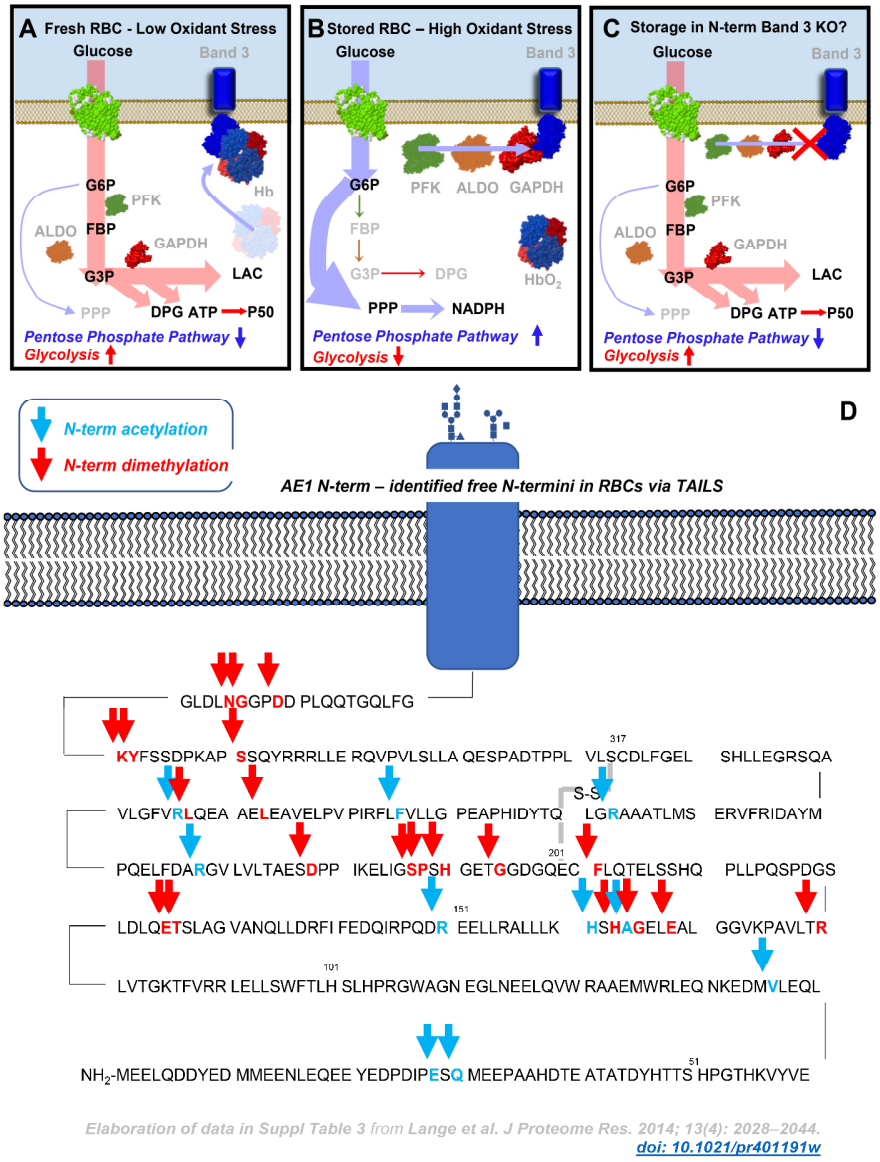

Supplementary Figure 1 – A schematic model of the band 3-dependent regulation of glycolysis and the pentose phosphate pathway, as proposed by Low's, Castagnola's, Xia's and Doctor's groups. At low oxygen saturation, deoxyhemoglobin binds to the N-term of band 3, while glycolytic enzymes are displaced from the same region and are active – resulting in increased fluxes through glycolysis and decreased fluxes through the pentose phospahte pathway (**A**). At high oxygen saturation, hemoglobin is displaced from the membrane and glycolytic enzymes bind to the N-term of band 3, resulting in their partial inhibition, decreases in fluxes through glycolysis and increased fluxes through the pentose phosphate pathway to generate the reducing equivalent NADPH necessary to counteract oxidant stress, which in turn increases as a function of Fenton chemistry in presence of oxygen (**B**). In **C**, in light of this model and the existing literature from our group and others, we predict that RBCs from mice lacking the N-term of band 3 would suffer from increased oxidant stress during storage under refrigerated conditions. We anticipate that RBCs from these mice would de facto phenocopy G6PD deficiency owing to the incapacity to redirect glucose oxidation fluxes towards the pentose phosphate pathway (**C**). In **D**, Re-elaboration of TAILS data from Lange et al. showing N-term band 3 residues that are fragmented at the end of the shelf-life of human packed red blood cells (storage day 42).

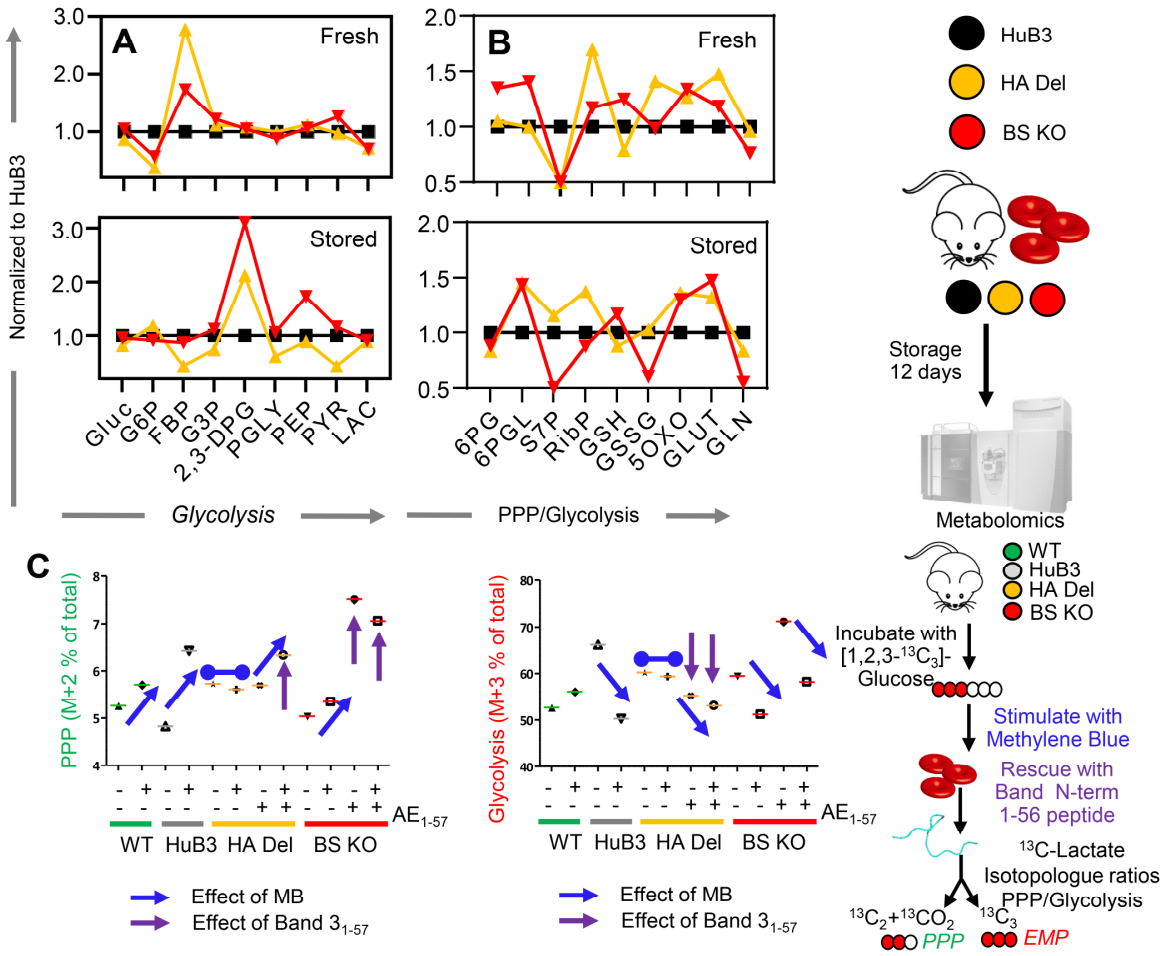

Supplementary Figure 2 – Alterations of glycolysis and the PPP in Band 3 KO mice and metabolic correlates to post-transfusion recovery in mice as gleaned by untargeted metabolomics analyses. Analyses of fresh and stored RBCs from wild type (C57BL6), humanized band 3 mice (HuB3) and mice lacking amino acids 1-11 (HA Del) or 12-23 (BS KO) of band 3 showed strain-specific differences in fresh and stored RBCs in glycolysis (**A**), pentose phosphate pathway (PPP) and glutathione homeostasis (**B**). Data in panels **A-B** report fold-change measurements in HA Del and BS KO mice normalized to the humanized band 3 mice (HuB3). To further investigate the impact on glycolysis and the PPP, RBCs from these four mouse strains were incubated with 1,2,3-13C3-glucose upon stimulation with methylene blue (MB). Rescue experiments were also performed by incubating RBCs with a recombinantly expressed N-term AE1 peptide (residues 1-57 - **C**), prior to determination of lactate isotopologues +3 and +2, deriving from glycolysis and the PPP, respectively (**C**).

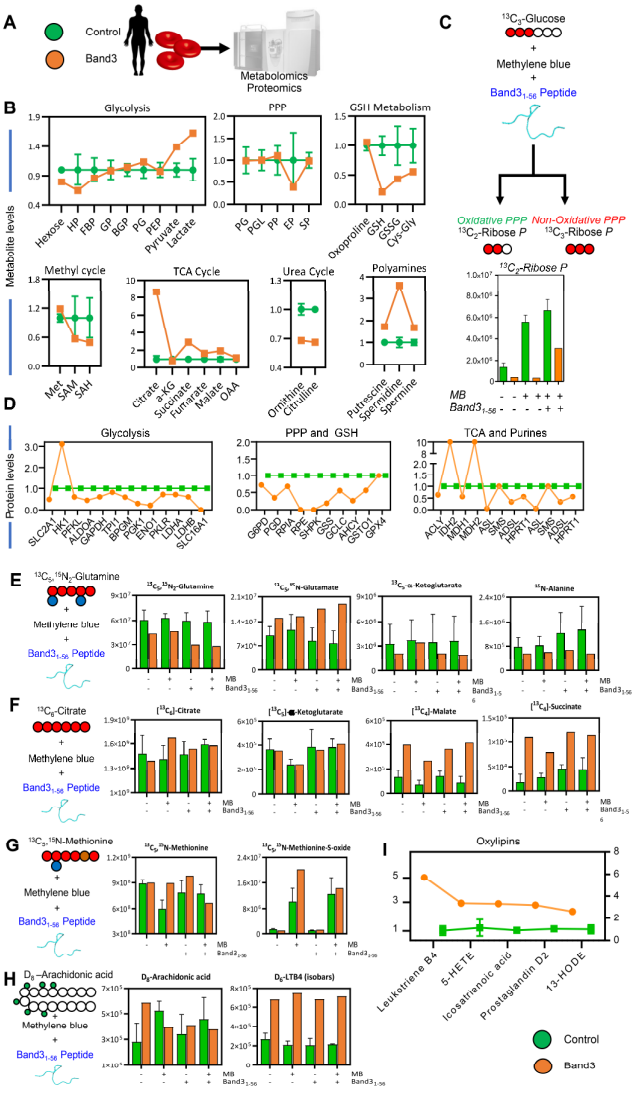

Supplementary Figure 3 – Metabolic impact of band 3 Neapolis in humans. Metabolomics and proteomics analyses were performed on RBCs from a male subject suffering from a genetic mutation resulting in the deletion of the first 11 amino acids of band 3, de facto phenocopying the high affinity deletion KO mice investigated in this study (**A**). Results highlight a significant alteration of glycolysis (increase), glutathione homeostasis (increased oxidant stress) and polyamine metabolism in this subject compared to healthy controls (n=3 – **B**). Incubation of band 3 Neapolis RBC lysates with 1,2,3-$^{13}C_3$-glucose confirmed a deficit in the capacity to activate the pentose phosphate following stimulation with methylene blue (MB), a defect that was corrected by rescue with a recombinantly expressed N-term of band 3 peptide (residues 1-57 – **C**). Proteomics analyses showed higher levels of hexokinase, but lower levels of all the remaining glycolytic enzymes downstream to it, as well as of enzymes of the pentose phosphate pathway and glutathione synthesis in the RBCs from the band 3 Neapolis individual (**D**). Tracing experiments with stable heavy isotope-labeled tracers ($^{13}C^{15}N$-glutamine – **E**; ^{13}C-citrate – **F**, $^{13}C^{15}N$-methionine – **G**, and deuterium labeled-arachidonate – **H**) confirmed alterations of glutaminolysis, carboxylic acid metabolism, isoaspartyl-damage repair via methylation and oxylipin metabolism (**I**) in the RBCs from the band 3 Neapolis subject – suggesting a role for band 3-dependent regulation of RBC metabolism beyond glycolysis and the pentose phosphate pathway. Specifically, increased consumption of labeled glutamine and generation of labeled glutamate, accompanied by decreases in labeled alpha-ketoglutarate and alanine are consistent with increased glutaminase activity and decreased transamination in RBCs from the band 3 Neapolis subject compared to controls (**E**). No significant differences were observed with respect to the levels of labeled citrate, or citrate-derived alpha-ketoglutarate (**F**). However, band 3 Neapolis RBCs had four-fold higher levels $^{13}C_4$-succinate and malate, in part explained by the higher degree of reticulocytosis in this subject (0.35x106/µl – **Supplementary Table 1**). None of the defects mentioned above was aggravated by treatment with MB or rescue with the recombinant AE11-56 peptide. Studies with labeled methionine showed significant methionine oxidation into its sulfoxide form, especially in response to MB, a defect that was normalized to control values following rescue with the AE11-56 peptide (**G**). Steady state levels of oxylipins were higher in the band 3 Neapolis RBCs compared to controls (**I**), which was confirmed by increased arachidonate metabolism in tracing experiments with deuterium-labeled arachidonic acid (**H**), consistent with what observed in band 3 KO mice.

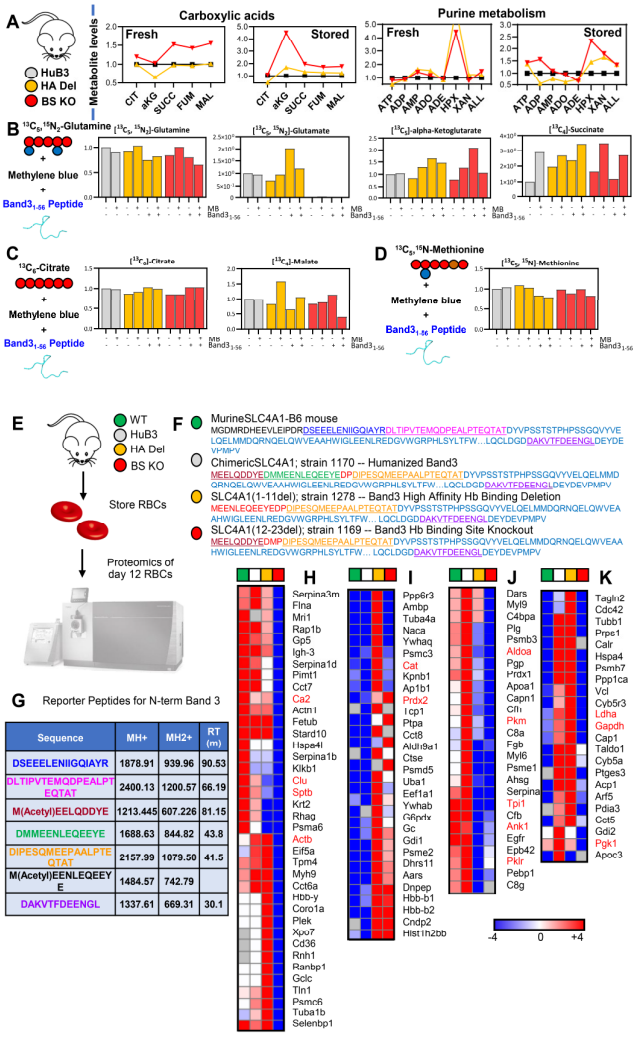

Sequence	MH+	MH2+	RT (m)
DSEEELENIIGQIAYR	1878.91	939.96	90.53
DLTIPVTEMQDPEALPTEQTAT	2400.13	1200.57	66.19
M(Acetyl)EELQDDYE	1213.445	607.226	81.15
DMMEENLEQEEYE	1688.63	844.82	43.8
DIPESQMEEPAALPTEQTAT	2157.99	1079.50	41.5
M(Acetyl)EENLEQEEYE	1484.57	742.79	
DAKVTFDEENGL	1337.61	669.31	30.1

Supplementary Figure 4 – Widespread metabolic alterations were observed in humanized Band 3 (HuB3) or band 3 KO mice lacking residues 1-11 (HA Del) or 12-23 (BS KO). Pathways affected included carboxylic acid and purine metabolism in fresh and stored RBCs (**A**). To further expand on these observations, tracing experiments with $^{13}C^{15}N$-glutamine (**B**), ^{13}C-citrate (**C**) and $^{13}C^{15}N$-methionine (**D**) were performed in RBCs from the three mouse strains, in presence or absence of pro-oxidant challenges with methylene blue (MB) and rescue with a recombinant version of the band 3 peptide (residues 1-56). **Proteomics characterization of RBCs from WT and Band 3 KO mice and thermal proteome profiling of recombinant peptide 1-56 of band 3 in RBC lysates.** Proteomics analyses were performed (**E**) to validate the lack of the N-term portion of band 3 in the KO mice (1-11 – highlighted in red - for HA Del; 12-23 – green – for BS KO; in black, peptides unique to the mouse N-term of band 3; in light blue, human band 3 sequence; underlined sequences represent peptides identified in these analyses – **F**). From these analyses, reporter peptide sequences were identified to screen for the four mouse strains through multiple reaction monitoring based approaches (**G**). Proteomics characterization of RBCs from the four mouse strains highlighted a significant impact of BS KO (**H**), either BS KO or HA Del (**I-J**) or HA Del alone (**K**) on several RBC proteins, including numerous well-established interactors of band 3 (highlighted in red in **H-K**).

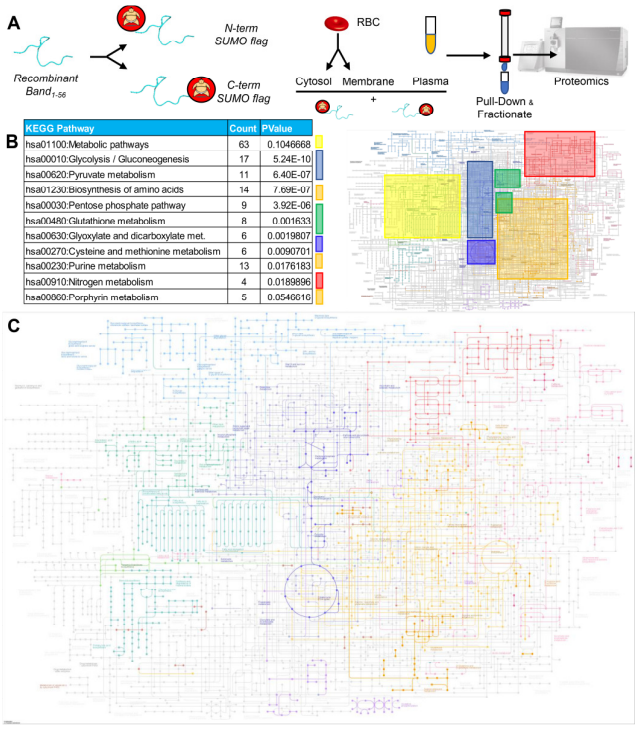

KEGG Pathway	Count	PValue
hsa01100:Metabolic pathways	63	0.1046668
hsa00010:Glycolysis / Gluconeogenesis	17	5.24E-10
hsa00620:Pyruvate metabolism	11	6.40E-07
hsa01230:Biosynthesis of amino acids	14	7.69E-07
hsa00030:Pentose phosphate pathway	9	3.92E-06
hsa00480:Glutathione metabolism	8	0.001633
hsa00630:Glyoxylate and dicarboxylate met.	6	0.0019807
hsa00270:Cysteine and methionine metabolism	6	0.0090701
hsa00230:Purine metabolism	13	0.0176183
hsa00910:Nitrogen metabolism	4	0.0189896
hsa00860:Porphyrin metabolism	5	0.0546016

Supplementary Figure 5 – Immuno-precipitation proteomics studies with recombinantly expressed band 3 1-56. A peptide coding for the amino acids 1-56 of the N-term of band 3 was recombinantly expressed with a SUMO-tag at either the N- or C-term terminus of the peptide, prior to incubation with plasma, red blood cell cytosols and membrane in independent experiments, pull-down against the SUMO tag, fractionation and nanoUHPLC-MS/MS-based identification of band 3 interacting partners (**A**). Pathway analyses of the hits from this analysis revealed a widespread interaction of band 3 with up to 63 proteins involved in metabolic regulation, as mapped against the KEGG pathway map of human metabolism (**B**). In **C,** enzymes identified from the pull down of SUMO-tagged band 3 1-56 mapped against the Metabolic pathways map (KEGG map: hsa01100).

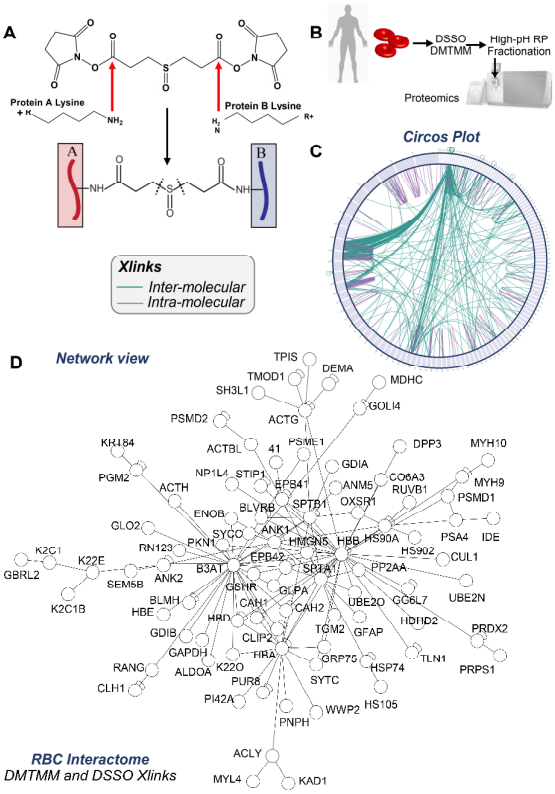

Supplementary Figure 6 – Red Blood Cell experimental interactome as gleaned by cross-linking proteomics experiments. In **A**, an overview of the cross-linking strategy with DSSO. This approach affords determination of protein-protein interactions by cross-linking free amines of adjacent residues of interacting proteins within a range spanning from 11.4 to 24 Å. In the present study, DSSO and DMTMM (E/D residues to K) were combined to investigate the RBC interactome (**B**). In **C**, circos plot view of the protein-protein cross-links identified in this study (full list in **Supplementary Table 1**). In **D**, the same inputs were used to provide a network view of the results.

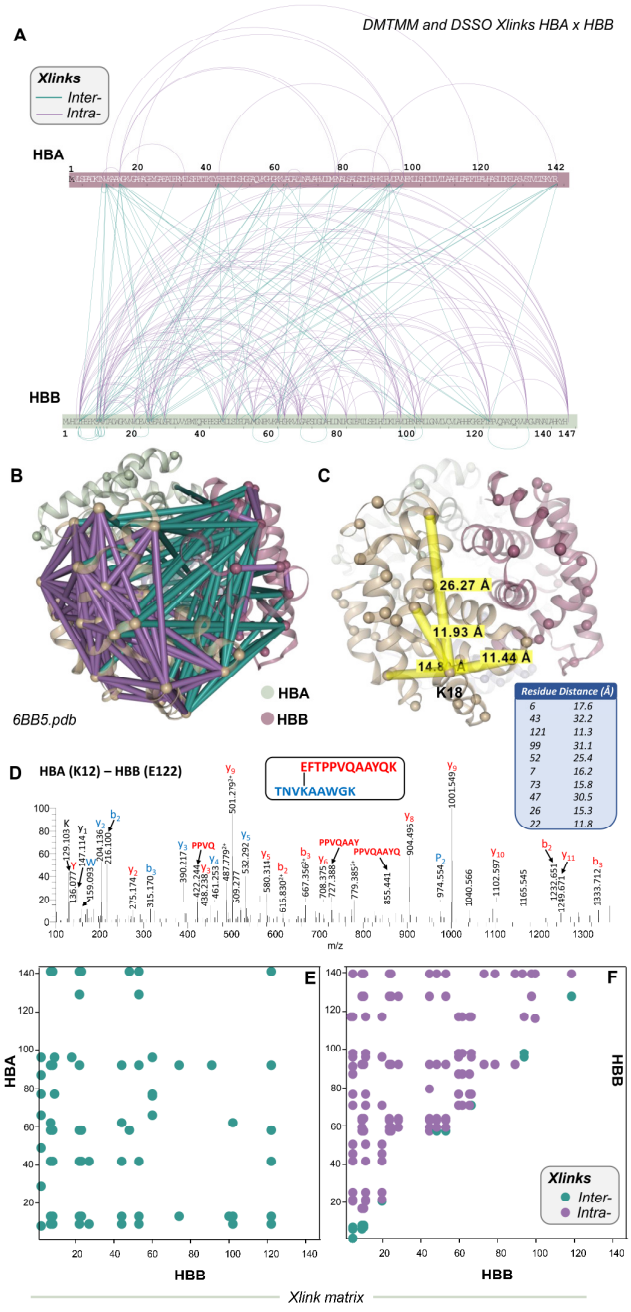

Supplementary Figure 7 – Cross-linking proteomics studies recapitulate structural elucidation of hemoglobin tetramers. In **A**, bar plots show the experimental intra (purple) or inter-molecular cross-links (teal) between alpha and beta hemoglobin chains (HBA and HBB), respectively. Based on these experimental data, cross-links were mapped against the structure of hemoglobin tetramers for human oxy-hemoglobin (6BB5.pdb – **B**). In **C**, highlighted cross-links and distances between K18 of HBA and neighboring residues. In **D**, a representative mass spectrum from MS3 analyses of one of the highest-scores cross-links, between the peptides containing K12 and E122 of HBA and HBB, respectively (y and b series ions are annotated). In **E** and **F**, matrix plots showing cross-links between HBA and HBB (teal) or within HBB (purple for intra and teal for inter-chain cross-links).

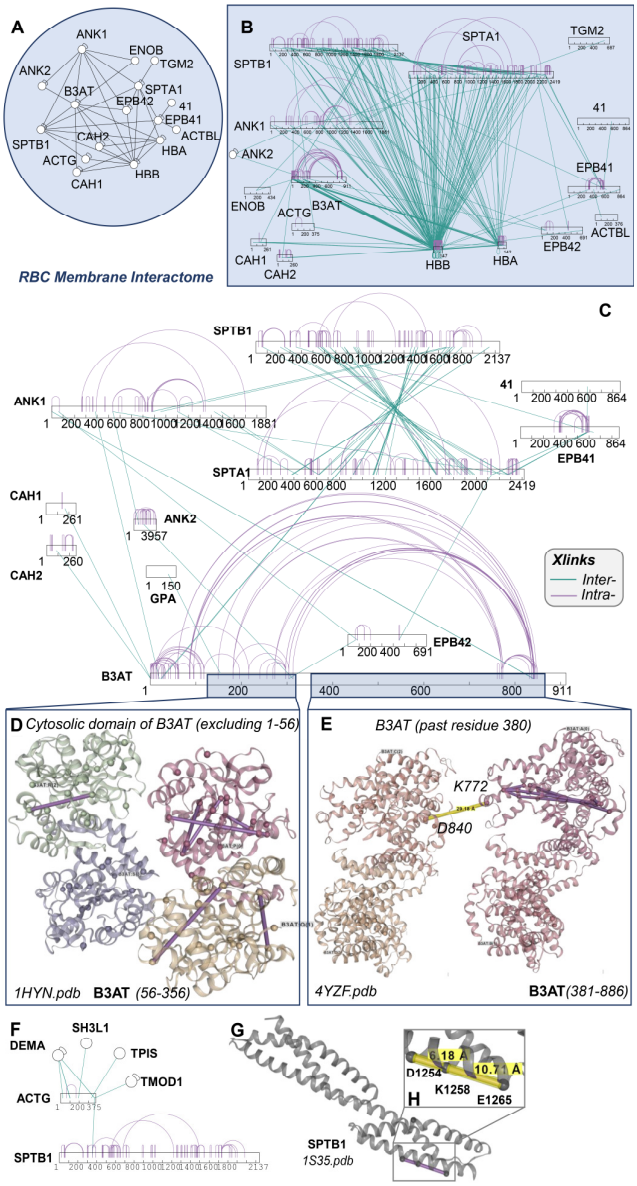

Supplementary Figure 8 – Experimental interactome of red blood cell membrane proteins. In **A**, highlighted network of RBC membrane proteins according to the canonical models (proteins are abbreviated as Uniprot gene names). In **B**, an overview of the interactions across these proteins in bar plot format. In **C**, expansion of the bar plots focusing on band 3 (B3AT), spectrin alpha and beta (SPTA1 and SPTB1), ankyrins 1 and 2 (ANK1 and ANK2), carbonic anhydrase 1 and 2 (CAH1 and CAH2), erythrocyte protein band 4.1 and 4.2 (41 and EPB42). In **D** and **E**, highlights of the intramolecular interaction of band 3 (residues 56-356 – *1HYN.pdb* and 381-886 – *4YZF.pdb,* respectively). In **F**, zoom in on a sub-network of structural proteins interacting with STPB1. Zoom in on a subset of intramolecular cross-links in SPTB1 (*1S35.pdb* – **G**) are shown in **H**.

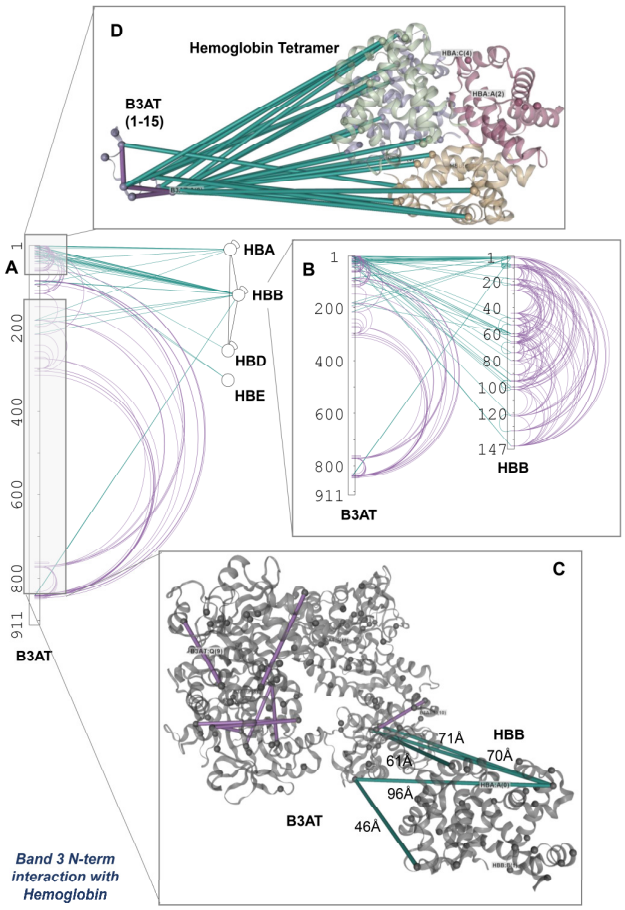

Supplementary Figure 9 – Cross-linking proteomics provides direct evidence of the interactions between hemoglobin and the N-terminus of band 3. These interactions are shown in bar plot format for band 3 (B3AT) with several hemoglobin chains (including alpha, beta, delta and epsilon – HBA, HBB, HBD and HBE - **A**), with a zoom on the cross-links between B3AT and HBB in **B**. In **C** and **D**, the interactions in **B** are highlighted against hemoglobin structure and B3AT cytosolic regions 1-15 and 56-356.

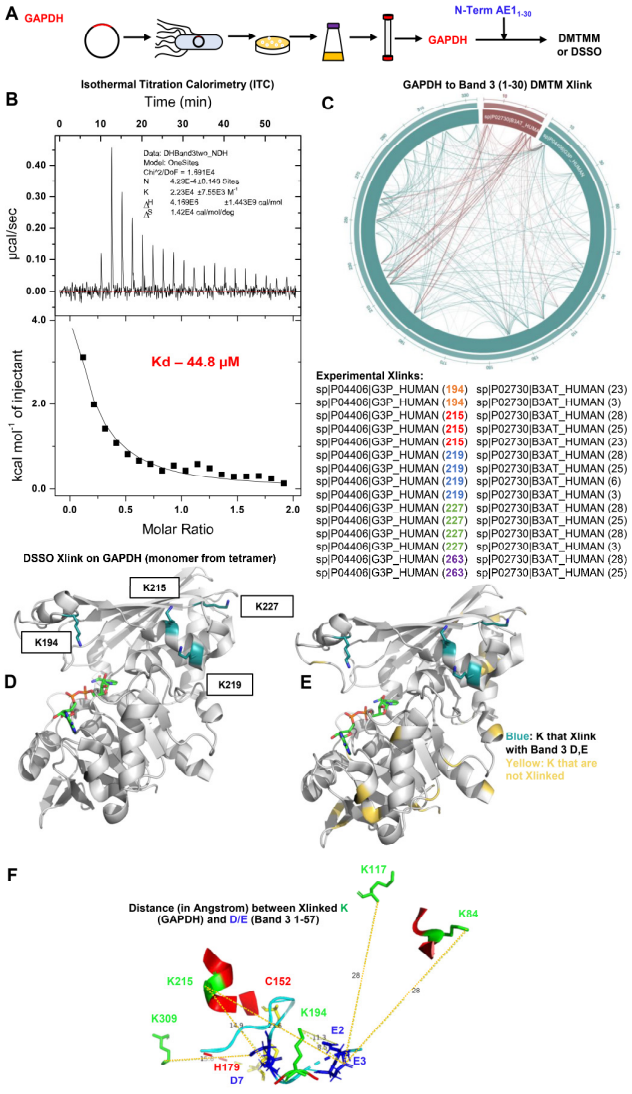

Supplementary Figure 10 – Recombinant expression of band 3 1-30 results in interaction with recombinant GAPDH (A) that have weaker interaction than AE1 1-56 (44.8 uM vs 2.56 uM). Cross-links with DMTMM are listed in **C** and DSSO cross-links on GAPDH with D/E on band 3 1-30 were mapped against GAPDH structure in **D-E**. In **F,** distance of cross-linked lysine (K – green) ε-amine side chain residues on glyceraldehyde 3-phosphate dehydrogenase and carboxylic acid side chains of glutamate/aspartate carboxylate residues on band 3 (residues 1-56 – no K is present on band 3 before residue 57) as experimentally determined by DSSO cross-linking proteomics.